CLINICAL AND EXPERIMENTAL
OPTOMETRY

REVIEW

Intraocular lens alignment from Purkinje and Scheimpflug imaging

Clin Exp Optom 2010 DOI:10.1111/j.1444-0938.2010.00514.x

Patricia Rosales*† PhD
Alberto de Castro* MSc
Ignacio Jiménez-Alfaro§ MD PhD
Susana Marcos* PhD
* Instituto de Óptica 'Daza de Valdés', Consejo Superior de Investigaciones Científicas, Madrid, Spain
† Centro de Investigaciones de la Armada, Madrid, Spain
§ Fundación Jiménez Díaz, Madrid, Spain
E-mail: susana@io.cfmac.csic.es

Submitted: 24 March 2010
Revised: 14 May 2010
Accepted for publication: 18 May 2010

The improved designs of intraocular lenses (IOLs) implanted during cataract surgery demand understanding of the possible effects of lens misalignment on optical performance. In this review, we describe the implementation, set-up and validation of two methods to measure *in vivo* tilt and decentration of IOLs, one based on Purkinje imaging and the other on Scheimpflug imaging. The Purkinje system images the reflections of an oblique collimated light source on the anterior cornea and anterior and posterior IOL surfaces and relies on the well supported assumption of the linearity of the Purkinje images with respect to IOL tilt and decentration. Scheimpflug imaging requires geometrical distortion correction and image processing techniques to retrieve the pupillary axis, IOL axis and pupil centre from the three-dimensional anterior segment image of the eye. Validation of the techniques using a physical eye model indicates that IOL tilt is estimated within an accuracy of 0.261 degree and decentration within 0.161 mm. Measurements on patients implanted with aspheric IOLs indicate that IOL tilt and decentration tend to be mirror symmetric between left and right eyes. The average tilt was 1.54 degrees and the average decentration was 0.21 mm. Simulated aberration patterns using custom models of the patients eyes, built using anatomical data of the anterior cornea and foveal position, the IOL geometry and the measured IOL tilt and decentration predict the experimental wave aberrations measured using laser ray tracing aberrometry on the same eyes. This reveals a relatively minor contribution of IOL tilt and decentration on the higher-order aberrations of the normal pseudophakic eye.

Key words: aberrations, aspheric surface, cataract surgery, computer eye models, customisation, decentration, intraocular lens, misalignment, optical quality, tilt

In recent years, there has been a growing interest in measuring the alignment (tilt and decentration) of intraocular lenses (IOLs) implanted during cataract surgery. The interest has been primarily motivated by the improved designs of the recent IOLs, which aim at compensating for the spherical aberration of the cornea (aspheric designs) or providing extended depth-of-focus (multifocal designs). IOL alignment effects could be of great relevance in the performance of accommodative IOL designs, which conceptually work by an axial displacement of the IOL in response to an accommodative effort. Questions of clinical interest arise: how do IOLs stabilise within the capsule? Can the alignment of the lens change over time, for example, due to capsular fibrosis? What is the effect of tilt and decentration of the IOL on optical performance?

Until recently most reports of IOL tilt and decentration were primarily observational and the estimates of lens tilt were obtained by presenting to the subject fixation targets at different eccentricities and determining the fixation angle that produces an overlap of Purkinje reflections from the anterior and posterior lens.[1] Some studies proposed a systematic method to measure lens tilt and dececentration based on a linear relation between the locations of the Purkinje images and rotation of the eye, tilt and decentration of the lens in patients with IOLs.[1,2] This methodology was validated and extensively used by Barry, Dunne and Kirschkamp[3–5] in several studies of the misalignment of the ocular components and was the basis for the instrument that we describe here.[6]

An alternative to Purkinje imaging is the use of direct imaging of the anterior segment of the eye, from the anterior cornea to the posterior surface of the lens, such as achieved in Scheimpflug imaging.[7–9] In Scheimpflug imaging a slit is projected on the eye (and rotated for 3-D imaging) and the image is formed on a CCD with a tilted image plane, which permits anterior segment images with a large depth-of-focus. The images need to be corrected for geometrical distortion (arising from the geometrical configuration of the system) and optical distortion (arising from diffraction of preceding ocular surfaces).[9] Measurements of the IOL tilt and decentration measured with Scheimpflug imaging have been reported in the clinical literature, although in these instruments optical distortion is presumably not corrected.[10–16] Custom correcting algorithms have been used in a report of IOL tilt and decentration of phakic lenses and measured with a refurbished Nidek Scheimpflug system, which is no longer commercially available.[17]

Here, we review the development (hardware and software), validation and measurements of two instruments based on Purkinje and Scheimpflug imaging, developed at the Visual Optics and Biophotonics Laboratory (Instituto de Óptica, Consejo Superior de Investigaciones Científicas). The first set-up provides phakometry and lens tilt and decentration measurements from the reflections of double or single light emitting diodes (LEDs) from the anterior cornea and anterior and posterior lens surfaces (Purkinje images). The second method is based on custom-developed processing routines of a commercial Scheimpflug instrument (Pentacam, by Oculus). In this paper, we review the methodology, the validation of the instruments using physical eye models, results of IOL alignment on patients implanted with state-of-the-art monofocal IOLs and the impact of the measured IOL tilt and decentration on the optical performance of pseudophakic eyes.

METHODS TO MEASURE IOL TILT AND DECENTRATION

Purkinje imaging method

Purkinje images are reflections of the light from anterior and posterior corneal surfaces (first and second Purkinje images, PI and PII, although PII is difficult to image because it is overlapped by PI), and from anterior and posterior crystalline lens surfaces (third and fourth Purkinje images, PIII and PIV). Purkinje images I, III and IV can be captured by imaging the eye's pupil, as they are formed close to the pupillary plane (particularly PI and PIV). PI and PIV are relatively near to each other, so they are approximately in the same plane of focus, while PIII image is formed in a different plane. Therefore, to visualise the three Purkinje images, the camera of a system for Purkinje image detection should be focused at different planes or a telecentric lens used to visualise the three Purkinje images in the same plane with the same magnification. Typically, illumination is performed off-axis to avoid overlapping of the images. One of the earlier studies by Wulfeck[18] described a system to image the third Purkinje image using infrared photography and established the basis of the current systems. Since then, several Purkinje imaging set-ups with increasing levels of sophistication have been described for phakometry, that is, the measurement of the crystalline lens surface radii of curvature.[19–25]

The Purkinje system that we present to measure tilt and decentration of the intraocular lenses is based on the assumption that there is a linear relationship between the positions of the Purkinje images and eye rotation, lens tilt and decentration.[2] The system requires knowledge of the geometry of the lens, which can be obtained either from the nominal information provided by the manufacturer or from phakometric measurements from the same instrument. In addition, the system can be used to measure natural crystalline lens alignment in phakic eyes. Other recent implementations for Purkinje imaging systems for alignment have been presented by Tabernero and colleagues[26] and Schaeffel.[27]

OPTICAL SET-UP

Figure 1 shows the implementation of the Purkinje imaging set-up at the Visual Optics and Biophotonics Lab (Instituto de Óptica, CSIC). A full description of the instrument can be found in an earlier publication.[6] The system has two collimated illuminating channels (for right and left eyes) provided with 880 nm LEDs, with light sources at an angle of ±12 degrees from the optical axis of the eye. Additionally, double LEDs close to the eye are used for phakometry. The imaging channel consists of an infrared-enhanced CCD camera provided with a telecentric lens focused at the pupil plane. A third channel projects a visual stimulus on a mini-display for foveal and eccentric fixations and a Badal system to correct for refractive error and to stimulate accommodation. The mini-display has SVGA resolution and allows presentation of multiple targets. Figure 2 shows an example of the Purkinje images collected in a patient implanted with an IOL.

ESTIMATION OF TILT AND DECENTRATION FROM PURKINJE IMAGES

The method to obtain lens tilt and decentration is based on that described by Phillips and co-workers[2] and other works.[3–5] This method assumes a linear relation between Purkinje image positions referred to the pupil centre $P1$, $P3$ and $P4$ and rotation of the eye β, tilt α and decentration d.

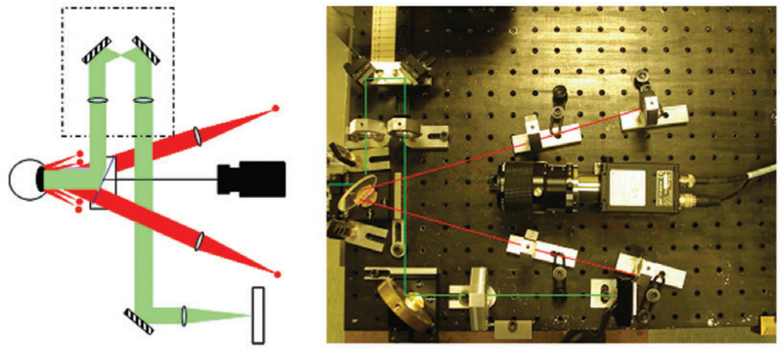

Figure 1. A Diagram of the Purkinje imaging system optical set-up. B. Photograph of the instrument at the Visual Optics and Biophotonics Lab, Instituto de Optica, CSIC.

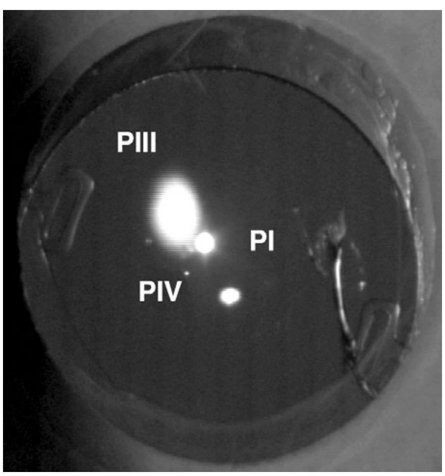

Figure 2. Example of pupillary images showing PI, PIII and PIV in a patient's eye implanted with an IOL

$$
\begin{aligned}
P1 &= E\beta \\
P2 &= F\beta + A\alpha + Cd \\
P3 &= G\beta + B\alpha + Dd
\end{aligned}
\qquad \textbf{(1)}
$$

To obtain the coefficients in these equations for each eye, we use simulated model eyes with spherical surfaces and the individual anatomical parameters available for each subject, using an optical design program (Zemax, Focus Software). To obtain coefficients *E*, *F* and *G*, in equation (1), we set $\alpha = 0$ and $d = 0$ (no tilt and no decentration) in the model eye. We estimated the Purkinje image positions for different rotation angles and we calculated coefficients *E*, *F*, *G* by linear fitting of the slope. The same procedure is repeated for *A* and *B* (setting $\beta = 0$ and $d = 0$) and C and D, (with $\beta = 0$ and $\alpha = 0$).

Scheimpflug imaging method

Scheimpflug imaging improves the slit-lamp geometry, by using the Scheimpflug principle. Normally, the lens and image (film or sensor) planes of a camera are parallel and the plane of focus is parallel to the lens and image planes (Figure 3A). If a planar object is also parallel to the image plane, it can coincide with the plane of focus and the entire subject can be rendered sharply. If the subject plane is not parallel to the image plane, it will be in focus only along a line where it intersects the plane of focus, as illustrated in Figure 3A. When an oblique tangent is extended from the image plane and another is extended from the lens plane, they meet at a point through which the plane of focus also passes, as illustrated in Figure 3B. With this condition, a planar subject that is not parallel to the image plane can be completely in focus.

The special geometry of the Scheimpflug configuration allows imaging the anterior segment with a large depth of focus but it introduces a geometrical distortion, because the magnification is not constant over the image. Additionally, because of the refraction from the different ocular surfaces, the Scheimpflug camera also introduces an optical distortion, due to the fact that each of the ocular surfaces is seen through the previous one (that is, the anterior lens is seen through the posterior and anterior cornea). To obtain reliable information from those images, those distortions must be corrected.[9] Distortion correction algorithms have been implemented for the Topcon SL-45 and the Nidek Eas-1000 Scheimpflug systems, which are no longer commercially available. We have recently published the implementation of geometrical and distortion correction algorithms for the Oculus Pentacam system.[28]

TILT AND DECENTRATION FROM SCHEIMPFLUG IMAGES

The Oculus Pentacam system was used to image the anterior segment of the eye in 25 different meridians. The commercial software included correction routines but only for the cornea.[29] In addition, the edge detection routines of the software fail to detect the edges of some IOLs with scattering properties very different from the crystalline lens (that is, acrylic). Therefore, the algorithms for the estimation of tilt and decentration of the intraocular lenses were applied directly to the raw images. The computational procedure to estimate tilt and decentration from the Scheimpflug images involved the following steps.

1. Correction of the geometrical distortion of the cross-sectional images, using a calibration reticule.
2. Edge detection of the cornea and IOL.
3. Calculation of IOL tilt and decentration in the cross-sectional images, estimating the pupil centre as the midpoint of the two visible pupil segments and the IOL centre as the midpoint of the intersection of the two spheres fitting anterior and posterior edges of the IOL, and the IOL as the line joining the centres of curvature of anterior and posterior surfaces of the IOL (see figure 4).
4. Calculation of IOL tilt and decentration in 3-D, by fitting the parameters calculated in step 3 at each of the 25

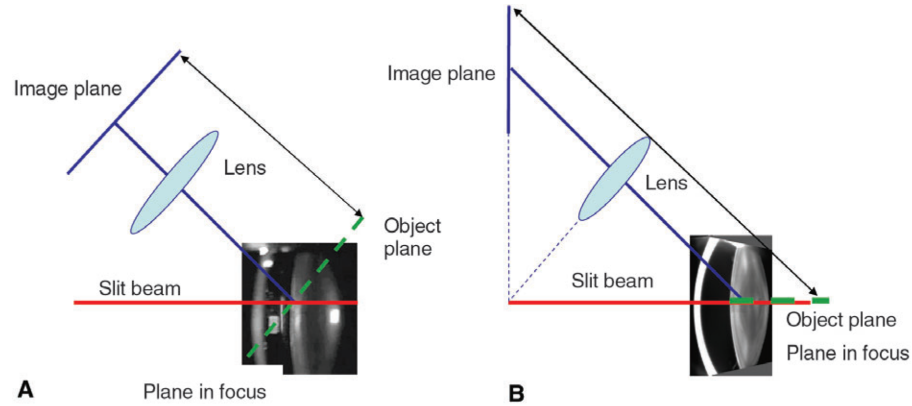

Figure 3. A. Principle of slitlamp imaging. A slit beam is focused on the eye and viewed with a microscope. The plane image and object image are parallel to each other. B. Principle of Scheimpflug imaging, where the image and objects planes are tilted with respect to each other in such a way that they intersect in one point.

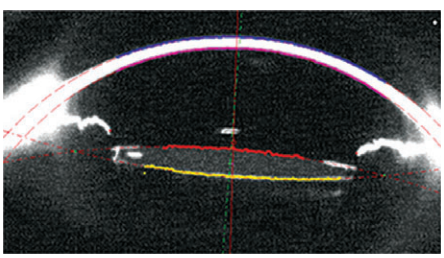

Figure 4. Raw image obtained from Scheimpflug camera in a pseudophakic eye. Edge detected points and circumferences fitting those points are superimposed. Centre of the pupil, centre of the IOL, pupil axis and IOL axis are shown.

meridional cross-sections to sinusoidal functions as a function of meridional angle. The horizontal and vertical pupil centres, the IOL centre, pupil axis and IOL axis are then computed evaluating the fitted sinusoidal function at 90 and 180 degrees. Decentration of the IOL is referred to the pupil centre and the tilt of the IOL is calculated by means of scalar product between pupillary and IOL axes.

An error analysis propagation assuming errors in edge detection was done and it showed an accuracy of 0.2 degrees in IOL tilt calculation and 0.01 mm in decentration provided that there are no optical distortions and no other sources of error.

Validation of the Purkinje and Scheimpflug method through a physical eye model

To validate the instruments, a physical model eye was built in which nominal values of tilt and decentration of the IOL can be set. It consists of a polymethyl methacrilate (PMMA) cell with water and a PMMA spherical contact lens (7.80 mm anterior radius and 6.48 mm posterior radius) simulating the cornea and an IOL at 5.0 mm behind the cornea. The IOL is mounted in a XYZ micrometer and rotatory stage. Three different IOLs from different manufacturers (Pharmacia, Alcon, Advanced Medical Optics) and powers (19, 22 and 26 dioptres) were mounted in the micrometer and rotatory stage. Nominal decentration ranged from zero to 2 mm, in steps of 1 mm, and nominal tilts ranged from zero to four degrees, in steps of one degree. A photograph of the model eye is shown in Figure 5A. Figures 5B and 5C show the estimated tilt and decentration from the Purkinje and Scheimpflug methods with respect to the nominal values set in the model eye averaged for the three IOLs used. On average, the discrepancy was 0.094 mm (Purkinje) and 0.228 mm (Scheimpflug) in decentration and 0.279 degree (Purkinje) and 0.243 degree (Scheipmflug) in tilt.

IOL TILT AND DECENTRATION MEASURED IN PATIENT EYES

The instruments described were used to measure tilt and decentration in 21 eyes from 12 patients (average age 72 ± 8 years) with implanted aspheric intraocular lenses (Tecnis, AMO, and AcrySof IQ, Alcon Research labs). Data from these patients have been reported previously.[6,30–32] Measurements were performed through pupils dilated with tropicamide 1%. Twenty-one eyes of 12 patients were measured in both systems. All protocols adhered to the declaration of Helsinki and followed protocols approved by the institutional review boards.

IOL tilt and decentration were estimated with respect to the pupillary axis (axis linking the centre of the pupil with the centre of curvature of the cornea) and the pupil centre, respectively. The centre of the pupil refers to the dilated pupil. Figure 6 shows a schematic diagram for the sign convention and definitions. Figure 7 shows tilt (A) and decentration (B) from Purkinje and Scheimpflug imaging in 12 pseudophakic patients. The data show clear mirror symmetry in tilt (as measured with both techniques) and a slightly less systematic trend for decentration in this group of eyes. In general, lens tilt does not exceed five degrees and lens decentration does not exceed five millimetres. We found average absolute tilts around X of 1.89 ± 1.00 degrees (Purkinje) and 1.17 ± 0.75 degrees (Scheimpflug), average absolute tilts around Y of 2.34 ± 0.97 degrees (Purkinje) and 1.56 ± 0.82 degrees (Scheimpflug), average absolute horizontal decentration of 0.34 ± 0.19 mm (Purkinje) and 0.23 ± 0.19 mm (Scheimpflug) and average absolute vertical decentration of 0.17 ± 0.23 mm (Purkinje) and 0.19 ± 0.20 mm (Scheimpflug).

In a previous study, we compared the estimates from both techniques in detail. Both techniques show a forward (toward the cornea) tilt of the nasal side of the

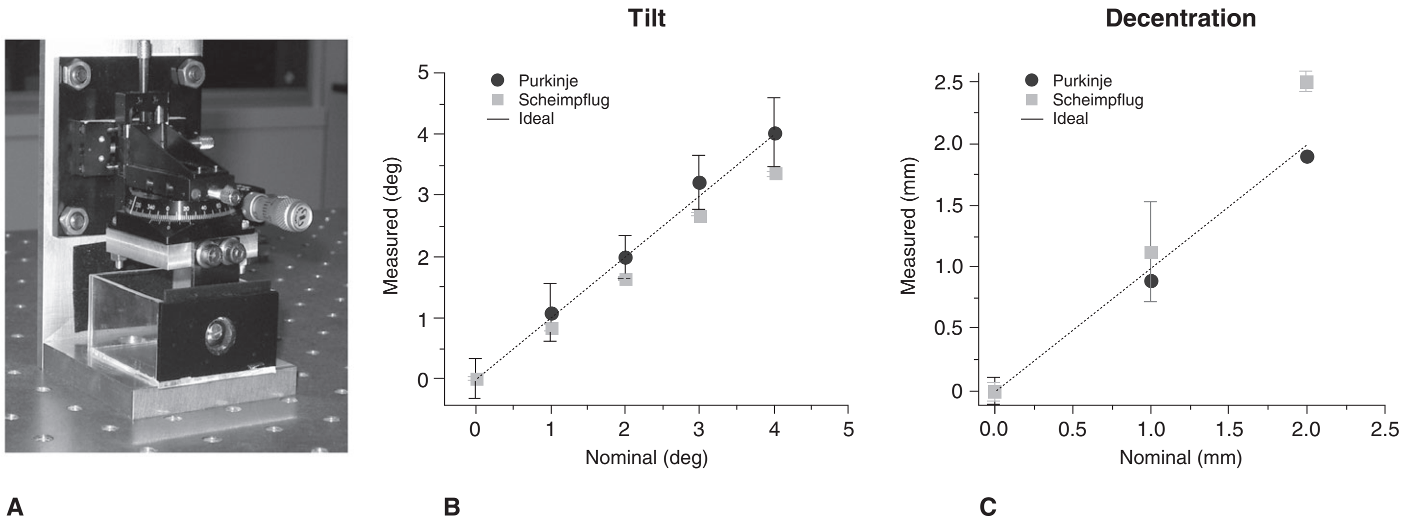

Figure 5. A. Photograph of the physical model eye used in the validations. B. Nomimal versus estimated tilt. C. Nominal versus estimated decentration. ● represents data from Purkinje and ■ from Scheimpflug. Results are the average of three IOLs. The ideal X = Y line is also plotted.

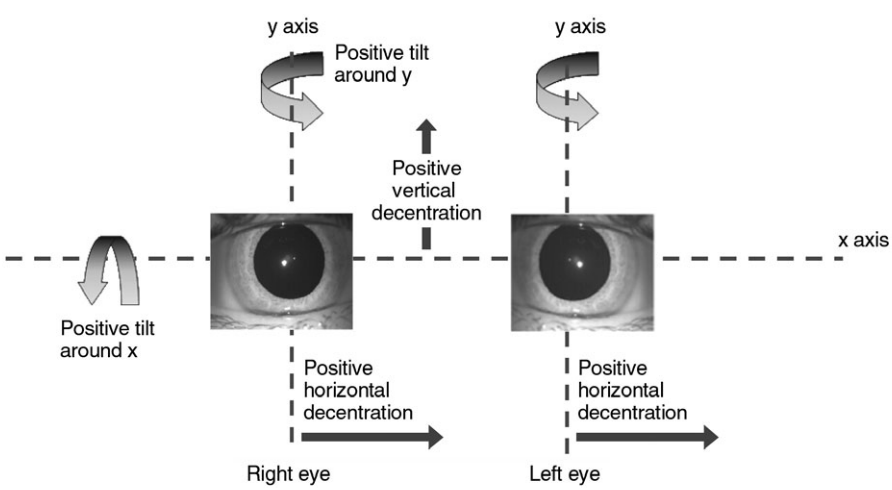

Figure 6. Schematic diagram for the sign conventions and definitions of tilt and decentration. Positive tilts around X-axis indicate that the superior edge of the IOL is moved forward and vice versa for negative tilts around X-axis. Positive tilts around Y-axis stand for nasal tilt and indicate that the nasal edge of the IOL is moved backwards and vice versa for a negative tilt around Y-axis, in right eyes. A positive tilt around Y-axis stands for temporal tilt (nasal edge of the IOL moves forward) in left eyes. A positive horizontal decentration stands for a nasal decentration in right eyes and temporal in left eyes. Positive vertical decentration indicates that the IOL is shifted upwards and vice versa for negative.

IOL, and a clear mirror horizontal symmetry of tilt across right and left eyes. Also, both techniques show a nasal displacement of the IOLs and a clear mirror horizontal symmetry of tilt across right and left eyes. Both techniques provide similar estimates for horizontal decentration (r = 0.764) and tilt around the Y-axis (r = 0.762), that is, horizontal displacements of the lens, for which both methods were found to be reliable from an intra-class correlation analysis. The mean average standard deviation of repeated measurements was 0.61 degree (Purkinje) and 0.20 degree (Scheimpflug) for tilt and 0.05 mm (Purkinje) and 0.09 mm (Scheimpflug) for decentration.

EFFECT OF IOL TILT AND DECENTRATION ON RETINAL IMAGE QUALITY

Decentration and tilt of the optical elements are expected to affect retinal image quality[33] and debates on the potential effects on tilt and decentration of aspheric IOLs have been raised since the aspheric designs were first proposed.[34] Since the first reports of optical aberrations of

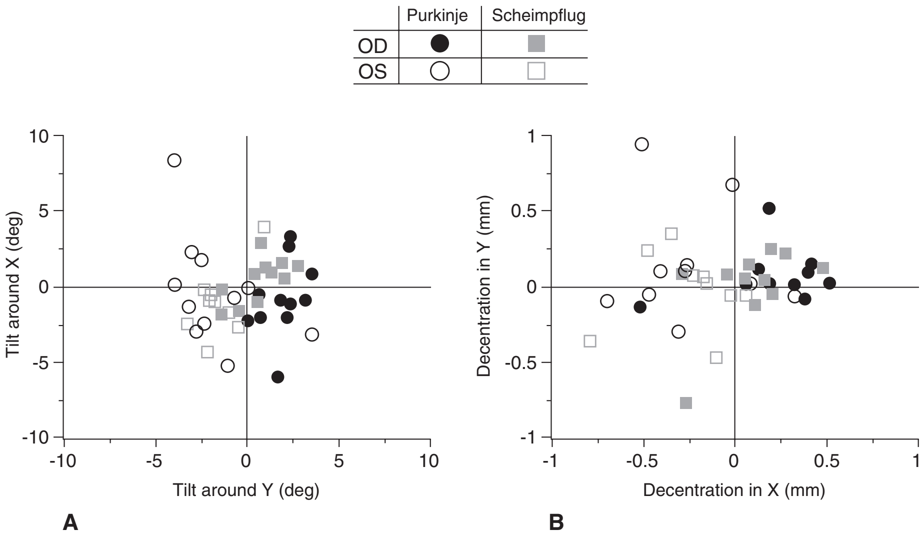

Figure 7. Tilt (A) and decentration (B) using Purkinje (●) and Scheimpflug (■) imaging. Solid symbols stand for right eyes and open symbols for left eyes. Refer to Figure 6 for sign conventions. The sign of the tilt around the X-axis has been changed to allow a more graphical representation of lens positioning, assuming a frontal view of the patients' eyes.

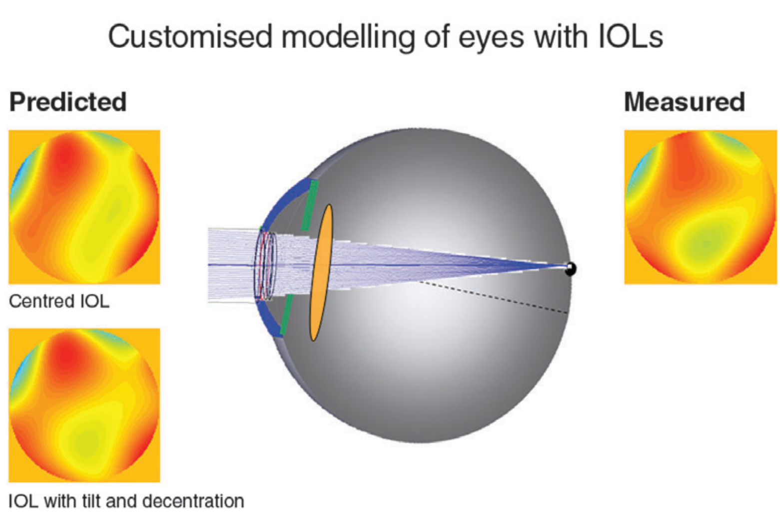

Figure 8. Schematic model eye as introduced in Zemax for numerical ray tracing and the different instruments used to obtain individual geometrical data (corneal elevation, anterior chamber depth ACD, IOL tilt and decentration) used in the model and to measure total aberrations. The wave aberration on the right represents that measured experimentally on one pseudophakic patient implanted with an aspheric IOL. The wave aberration patterns on the left represent simulations using a customised eye model for that patient's eye, assuming no tilt or decentration in the IOL (upper pattern) and the measured tilt and decentration of the IOL (lower pattern).

intraocular lenses *in vivo* in pseudophakic patients, there have been numerous studies of the optical aberrations with different types of IOLs.[35–39] Computer eye models are an excellent tool to identify the relative contribution of different factors that affect optical quality in pseudophakic eyes, which is helpful to evaluate the real impact of new IOL designs and the potential need to improve cataract surgery.

Most theoretical studies have concentrated on the impact of lens geometry on spherical aberration and the effect of tilt and decentration of the intraocular lens has been discussed based on theoretical models.[40,41] Computer eye models can be predictive only if actual anatomical values are used. In particular, it is important to incorporate the real amounts of tilt and decentration (along with their actual signs and combinations), the tilt of the line of sight (angle lambda),[32] the post-operative corneal topography,[31,42,43] the intraocular lens geometry and optical biometry.

We developed a customised model eye in patients with aspheric IOLs of known geometry, where tilt and decentration values have been measured *in vivo*. Experimental measurements of ocular aberrations (using a laser ray tracing technique[44–47]) in these eyes are compared with estimates of aberrations from numerical ray tracing using a customised model eye, with individual measurements of post-operative anatomical data, including IOL misalignment. The accuracy of customised eye models to predict measured aberrations[31,48] and their capability to investigate the contribution of the different components to overall image quality in eyes with IOLs and to assess the real benefits of new IOL designs have been demonstrated.[31]

Customised eye models were built using the Zemax (Focus Software, Tucson, AZ, Zemax) optical design program, where an optical system is defined as a sequential group of surfaces separated by refractive index media. The anterior corneal surface was obtained from videokeratoscopy while the posterior corneal surface was assumed to be a standard spherical surface with a radius of 6.5 mm. Corneal refractive index

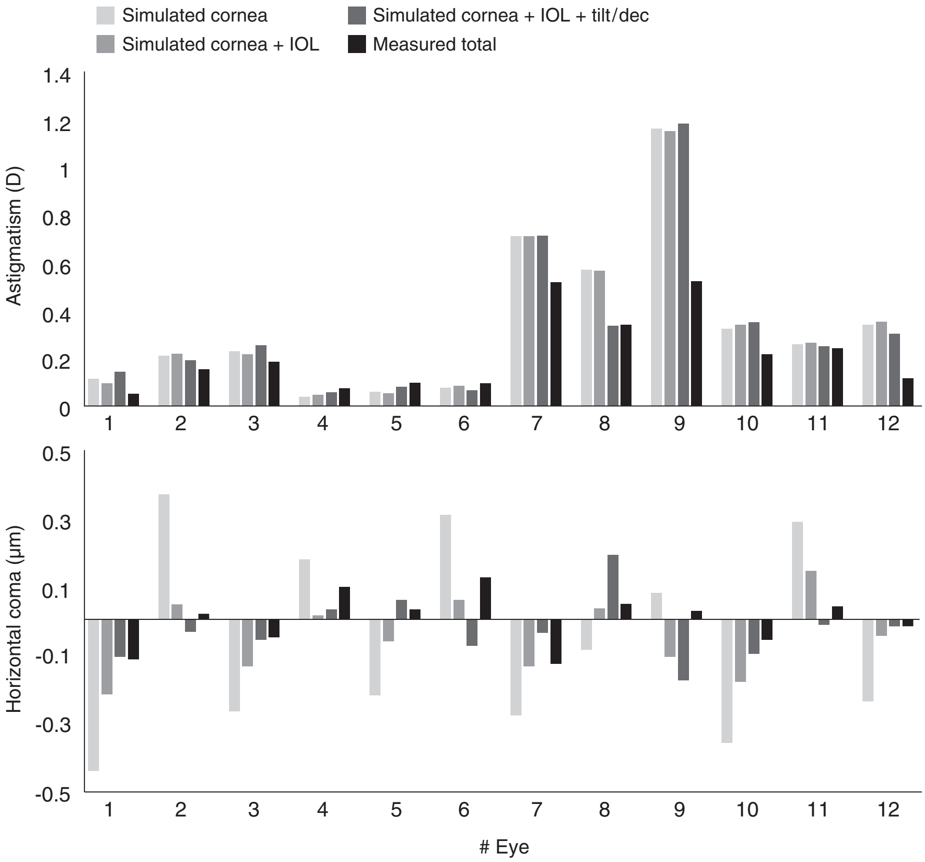

Figure 9. Top. Astigmatism. Bottom. Horizontal coma obtained for the real eyes and simulations with customised computer eyes (assuming the cornea and the IOL are centred, and the cornea and the IOL have real amounts of tilt and decentration).

was taken as 1.376. The IOL anterior and posterior surface geometry was provided by the manufacturer and introduced in the model eye as standard conic surfaces, with the nominal thickness and refractive index of the lens. Values of tilt and decentration of the IOL measured with the Purkinje imaging system were introduced with respect to the pupillary axis. Finally, the whole eye was rotated to simulate off-axis measurements obtained due to the eccentric location of the fovea (which is also estimated with Purkinje imaging for foveal fixation).

Figure 8 shows the schematic diagram of the customised model eye introduced in Zemax (for a wavelength of 786 nm) for the simulations and the different instruments used to measure corneal shape, ocular biometry, lens tilt and decentration, ocular aberrations and the measured total aberration pattern (higher-order aberrations) using LRT and simulations of the total wave aberration patterns for the same patient. The figure shows the predicted wave aberration assuming that the IOL is centred on the pupillary axis (zero tilt and decentration) or with the actual amount of measured tilt and decentration. The experimental wave aberration is well predicted by the estimated aberration from the customised model eye. A comparison between the predictions with and without IOL tilt and decentration indicates a minor role of IOL misalignment in the optical quality on this patient.

The same effects as those of the example in Figure 8 were found in all 12 patients of the study,[31] namely, a major role of the corneal aberrations, low amounts of spherical aberration (as a result of the aspheric design of the IOL) and minor role of IOL tilt and decentration.

While it is not expected that IOL tilt and decentration affect the amounts of total spherical aberration, it has been suggested that IOL misalignment may have a negative impact on astigmatism and coma. We showed that the differences in astigmatism and particularly coma are minor between the cases of centred or misaligned IOL. Figure 9A shows corneal astigmatism in the 12 eyes of the study, along with total astigmatism with the centred or misaligned IOL (computed using a customised model eye for each patient). The presence of IOL tilt and decentration nominally produced an increase in the astigmatism in six eyes and a decrease in five eyes. A relevant feature is the systematic overestimation of astigmatism (by 13 per cent on average) in the computer model eye with respect to the real eye, indicating the presence of a compensatory effect in the posterior corneal surface (which is not optimally simulated by a spherical surface).[49,50] Figure 9B shows corneal horizontal and total horizontal coma for the simulated and real eyes. Horizontal coma is reduced in all eyes with respect to corneal values, as shown by both simulated and real data (with a decrease between five and 35 per cent) and this is a result of passive compensation of the coma arising from foveal misalignment and which occurs with aspheric IOLs.[32] In addition, we found that the presence of real amounts and combinations of IOL tilt and decentration does not induce additional coma. In most eyes (seven of 12) the presence of tilt and decentration reduces horizontal coma (by 10 per cent) with respect to the simulation with a centred IOL. The systematic reduction of horizontal coma in the eye (shown both in the real measurements and simulations) arises from a passive balance between corneal coma (resulting from the misalignment of the fovea) and the internal aberration of opposite sign with aspheric IOLs.[32]

CONCLUSIONS

Purkinje and Scheimpflug imaging are valuable techniques to measure *in vivo* IOL tilt and decentration in pseudophakic patients.

The Purkinke imaging system captures reflections from the anterior cornea (PI) and anterior and posterior lens (PIII and PIV). IOL alignment is obtained from linear relationships between the Purkinje image positions and IOL tilt, decentration and ocular alignment.

Scheimpflug imaging works by projection of a (rotating) slitlamp onto the eye. The tilt of the image plane allows a large depth-of-focus in the anterior segment images. Distortions must be corrected before quantitative information is extracted from the image. Tilt and decentration can be obtained from Scheimpflug images using edge detection and curve fitting algorithms that allow estimation of the pupillary axis (defined as the reference) and the IOL axis.

Validations using physical eye models indicate that Purkinje and Scheimpflug images provide estimates of IOL decentration within an accuracy of 0.026 mm and IOL tilt within an accuracy of 0.6 degrees.

In a group of 12 patients implanted with aspheric IOLs, we found average absolute tilts around X of 1.89 ± 1.00 degrees (Purkinje) and 1.17 ± 0.75 degrees (Scheimpflug), average absolute tilts around Y of 2.34 ± 0.97 degrees (Purkinje) and 1.56 ± 0.82 degrees (Scheimpflug) and average absolute horizontal decentration of 0.34 ± 0.19 mm (Purkinje) and 0.23 ± 0.19 mm (Scheimpflug) and average absolute vertical decentration of 0.17 ± 0.23 mm (Purkinje) and 0.19 ± 0.20 mm (Scheimpflug). These amounts are similar to those found in natural crystalline lenses of phakic eyes. In addition, there was significant mirror symmetry in IOL alignment between right and left eyes.

Customised computer eye models of pseudophakic eyes (with individual data of corneal topography, lens geometry, lens tilt, lens decentration and fovea misalignment) predict the higher-order aberrations of pseudophakic eyes.

The contribution of lens tilt and decentration to optical quality degradation is relatively minor. In 60 per cent of the cases, the presence of lens tilt and decentration contributed favourably to the prediction of higher-order aberrations (with respect to the centred case).

GRANTS AND FINANCIAL ASSISTANCE
The authors acknowledge funding from MICINN FIS2008-02065 to Susana Marcos; EURYI-05-102-ES (EURHORCs-ESF) to Susana Marcos; FIS2005-04382 Predoctoral Fellowship to Patricia Rosales and CSIC I3P Program to Alberto de Castro.

REFERENCES

1. Guyton DL, Uozato H, Wisnicki HJ. Rapid determination of intraocular lens tilt and decentration trough the undilated pupil. *Ophthalmology* 1990; 97: 1259–1264.
2. Phillips P, Perez-Emmanuelli J, Rosskothen HD, Koester CJ. Measurement of intraocular lens decentration and tilt in vivo. *J Cataract Refract Surg* 1988; 14: 129–135.
3. Barry JC, Dunne M, Kirschkamp T. Phakometric measurement of ocular surface radius of curvature and alignment: evaluation of method with physical model eyes. *Ophthalmic Physiol Opt* 2001; 21: 450–460.
4. Barry JC, Branmann K, Dunne MCM. Catoptric properties of eyes with misaligned surfaces studied by exact ray tracing. *Invest Ophthalmol Vis Sci* 1997; 38: 1476–1484.
5. Kirschkamp T, Dunne M, Barry JC. Phakometric measurement of ocular surface radii of curvature, axial separations and alignment in relaxed and accommodated human eyes. *Ophthalmic Physiol Opt* 2004; 24: 65–73.
6. Rosales P, Marcos S. Phakometry and lens tilt and decentration using a custom-developed Purkinje imaging apparatus: validation and measurements. *J Opt Soc Am A Opt Image Sci Vis* 2006; 23: 509–520.
7. Brown N. The change in lens curvature with age. *Exp Eye Res* 1974; 19: 175–183.
8. Koretz J, Cook C, Kaufman P. Aging of the human lens: changes in lens shape at zero-diopter accommodation. *J Opt Soc Am A* 2001; 18: 265–272.
9. Dubbelman M, Van der Heijde GL. The shape of the aging human lens: curvature, equivalent refractive index and the lens paradox. *Vision Res* 2001; 41: 1867–1877.
10. Sasaki K, Sakamoto Y, Shibata T, Nakaizumi H, Emori Y. Measurement of postoperative intraocular lens tilting and decentration using Scheimpflug images. *J Cataract Refract Surg* 1989; 15: 454–457.
11. Hayashi K, Hayashi H, Nakao F, Hayashi F. Comparison of decentration and tilt between one piece and three piece polymethyl methacrylate intraocular lenses. *Br J Ophthalmol* 1998; 84: 419–422.
12. Wang MC, Woung LC, Hu CY, Kuo HC. Position of poly(methyl methacrylate) and silicone intraocular lenses after phacoemulsification. *J Cataract Refract Surg* 1998; 12: 1652–1657.
13. Jung CK, Chung SK, Baek NH. Decentration and tilt: silicone multifocal versus acrylic soft intraocular lenses. *J Cataract Refract Surg* 2000; 26: 582–585.
14. Kim JS, Shyn KH. Biometry of 3 types of intraocular lenses using Scheimpflug photography. *J Cataract Refract Surg* 2001; 27: 533–536.
15. Nejima R, Miyata K, Honbou M, Tokunaga T, Tanabe T, Sato M, Oshika T. A prospective, randomised comparison of single and three-piece acrylic foldable intraocular lenses. *Br J Ophthalmol* 2004; 88: 727–728.
16. Baumeister M, Neidhardt B, Strobel J, Kohnen T. Tilt and decentration of three-piece foldable high-refractive silicone and hydrophobic acrylic intraocular lenses with 6-mm optics in an intraindividual comparison. *Am J Ophthalmol* 2005; 104: 1051–1058.
17. Coppens JE, van den Berg TJ, Budo CJ. Biometry of phakic intraocular lens using Scheimpflug photography. *J Cataract Refract Surg* 2005; 31: 1904–1914.
18. Wulfeck J. Infrared photography of the so-called third Purkinje image. *J Opt Soc Am* 1955; 45: 928–930.
19. Van Veen H, Goss D. Simplified system of Purkinje image photography for phakometry. *Am J Optom Physiol Opt* 1998; 65: 905–908.
20. Sorsby A, Benjamin B, Sheridan M, Stone J, Leargy G. Refraction and its components during the growth of the eye from the age of three. *Memo Med Res Counc* 1961; 301: 1–67.
21. Mutti D, Zadnik K, Adams A. A video technique for phakometry of the human crystalline lens. *Invest Ophthalmol Vis Sci* 1992; 33: 1771–1782.
22. Smith G, Garner LF. Determination of the radius of curvature of the anterior lens surface from the Purkinje images. *Ophthalmic Physiol Opt* 1996; 16: 135–143.
23. Garner LF. Calculation of the radii of curvature of the crystalline lens surfaces. *Ophthalmic Physiol Opt* 1997; 17: 75–80.
24. Zadnik K, Mutti DO, Mitchell GL, Jones LA, Burr D, Moeschberger ML. Normal eye growth in emmetropic schoolchildren. *Optom Vis Sci* 2004; 81: 819–828.
25. Rosales P, Wendt M, Marcos S, Glasser A. Changes in the crystalline radii of curvature and lens tilt and decentration during

dynamic accommodation in Rhesus monkeys. *J Vision* 2008; 8: 1–12.
26. Tabernero J, Benito A, Nourrit V, Artal P. Instrument for measuring the misalignments of ocular surfaces. *Optics Express* 2006; 14: 10945–10956.
27. Schaeffel F. Binocular lens tilt and decentration measurements in healthy subjects with phakic eyes. *Invest Ophthalmol Vis Sci* 2008; 49: 2216–2222.
28. Rosales P, Marcos S. Pentacam Scheimpflug quantitative imaging of the crystalline lens and intraocular lens. *J Refract Surg* 2009; 25: 421–428.
29. Pérez-Escudero A, Dorronsoro C, Sawides L, Remón L, Merayo-Lloves J, Marcos S. Minor influence of myopic laser *in situ* keratomileusis on the posterior corneal surface. *Invest Ophthalmol Vis Sci* 2009; 50: 4146–4154.
30. de Castro A, Rosales P, Marcos S. Tilt and decentration of intraocular lenses in vivo from Purkinje and Scheimpflug imaging: validation study. *J Cataract Refract Surg* 2007; 33: 418–429.
31. Rosales P, Marcos S. Customized computer models of eyes with intraocular lenses. *Optics Express* 2007; 15: 2204–2218.
32. Marcos S, Rosales P, Llorente L, Barbero S, Jiménez-Alfaro I. Balance of corneal horizontal coma by internal optics in eyes with intraocular artificial lenses: evidence of a passive mechanism. *Vision Res* 2008; 48: 70–79.
33. Artal P, Marcos S, Iglesias I, Green DG. Optical modulation transfer function and contrast sensitivity with decentered small pupils. *Vision Res* 1996; 6: 3575–3586.
34. Atchison DA. Optical design of intraocular lenses. 1. On-axis performance. *Optom Vis Sci* 1989; 66: 492–506.
35. Barbero S, Marcos S, Jimenez-Alfaro I. Optical aberrations of intraocular lenses measured *in vivo* and *in vitro*. *J Opt Soc Am A* 2003; 20: 1841–1851.
36. Marcos S, Barbero S, Jiménez-Alfaro I. Optical quality and depth-of-field of eyes implanted with spherical and aspheric intraocular lenses. *J Refract Surg* 2005; 21: 223–235.
37. Mester U, Dillinger P, Anterist N. Impact of a modified optic design on visual function: clinical comparative study. *J Cataract Refract Surg* 2003; 29: 653–660.
38. Rocha KM, Soriano ES, Chalita MR, Yamada AC, Bottós J, Bottós J, Morimoto L *et al*. Wavefront analysis and contrast sensitivity of aspheric and spherical intraocular lenses: a randomized prospective study. *Am J Ophthalmol* 2006; 142: 750–756.
39. Rekas M, Krix-Jachym K, Zelichowska B, Ferrer-Blasco T, Montés-Micó R. Optical quality in eyes with aspheric intraocular lenses and in younger and older adult phakic eyes: comparative study. *J Cataract Refract Surg* 2009; 35: 297–302.
40. Atchison DA. Design of aspheric intraocular lenses. *Ophthalmic Physiol Opt* 1990; 11: 137–146.
41. Holladay J, Piers P, Koranyi G, van der Mooren M, Norrby N. A new intraocular lens design to reduce spherical aberration of pseudophakic eyes. *J Refract Surg* 2002; 18: 683–691.
42. Pesudovs K. Involvement of neural adaptation in the recovery of vision after laser refractive surgery. *J Refract Surg* 2005; 21: 144–147.
43. Guirao A, Tejedor J, Artal P. Corneal aberrations before and after small-incision cataract surgery. *Invest Ophthalmol Vis Sci* 2004; 45: 4312–4319.
44. Moreno-Barriuso E, Navarro R. Laser ray tracing versus Hartmann-Shack sensor for measuring optical aberrations in the human eye. *J Opt Soc Am A* 2000; 17: 974–985.
45. Marcos S, Díaz-Santana L, Llorente L, Dainty C. Ocular aberrations with ray tracing and Shack-Hartmann wavefront sensors: does polarization play a role? *J Opt Soc Am A* 2002; 19: 1063–1072.
46. Moreno-Barriuso E, Marcos S, Navarro R, Burns SA. Comparing laser ray tracing, spatially resolved refractometer and Hartmann-Shack sensor to measure the ocular wavefront aberration. *Optom Vis Sci* 2001; 78: 152–156.
47. Llorente L, Diaz-Santana L, Lara-Saucedo D, Marcos S. Aberrations of the human eye in visible and near infrared illumination. *Optom Vis Sci* 2003; 80: 26–35.
48. Tabernero J, Piers P, Benito A, Redondo M, Artal P. Predicting the optical performance of eyes implanted with IOLs to correct spherical aberration. *Invest Ophthalmol Vis Sci* 2006; 47: 4651–4658.
49. Dunne M, Royston J, Barnes D. Posterior corneal surface toricity and total corneal astigmatism. *Optom Vis Sci* 1991; 68: 708–710.
50 Dubbelman M, Sicam V, Van der Heijde GL. The shape of the anterior and posterior surface of the aging human cornea. *Vision Res* 2006; 46: 993–1001.

Corresponding author:
Dr Susana Marcos
Instituto de Optica 'Daza de Valdés'
Consejo Superior de Investigaciones Científicas
Serrano 121
28006 Madrid
SPAIN
E-mail: susana@io.cfmac.csic.es